HOKKAIDO UNIVERSITY

Title	Strength Deterioration of Nonfractal Particle Aggregates in Simple Shear Flow
Author(s)	Horii, Kento; Yamada, Reiko; Harada, Shusaku
Citation	Langmuir, 31(29), 7909-7918 https://doi.org/10.1021/acs.langmuir.5b00197
Issue Date	2015-07
Doc URL	http://hdl.handle.net/2115/62613
Rights	This document is the unedited Author's version of a Submitted Work that was subsequently accepted forpublication in Langmuir, copyright © American Chemical Society after peer review. To access the final edited and published work see http://pubs.acs.org/doi/abs/10.1021/acs.langmuir.5b00197
Type	article (author version)
File Information	langmuir.31(2015).7909-7918.pdf

Instructions for use

Hokkaido University Collection of Scholarly and Academic Papers : HUSCAP

Strength deterioration of non-fractal particle aggregate in simple shear flow

Kento Horii[†], Reiko Yamada[‡] and Shusaku Harada[*†]

[†] *Division of Sustainable Resources Engineering, Faculty of Engineering, Hokkaido University*

[‡] *Graduate School of Engineering, Nagasaki University*

E-mail: harada@eng.hokudai.ac.jp

Abstract

The restructuring of a non-fractal particle aggregate in simple shear flow was simulated by Stokesian dynamics approach. We studied the deformation and the resultant strength change of aggregate by surrounding flow under the condition that the cohesive strength of aggregate is comparable with the fluid stress. In particular, we focused on how the aggregate deteriorates due to the fluid stress exerted on it periodically. The image analysis was applied to visualized simulation results for quantitative estimation of irreversible change in aggregate configuration. We examined the structural change of aggregate from various perspectives, i.e., the outer shape, the internal strength and the fluid stress on the surface of the aggregate. The simulation results show that the aggregate gets squashed after intricate restructuring process and it elongates along with streamline as experimentally observed in the previous study. Regarding the internal strength, the weakest point locally develops in the aggregate by periodically-varying fluid stress. Combination of rotation and elongation effects of shear flow is complexly-involved in the deterioration of internal strength of aggregate.

[*] Corresponding author
[†] Address: N13W8, Sapporo, Hokkaido, 060-8628, Japan
[‡] Address: 1-14, Bunkyo, Nagasaki 852-8521, Japan

Introduction

Dispersion of colloidal aggregate in fluid flow has been of particular interest to many researchers in various engineering fields. Quantitative prediction of dispersion state such as size distribution of aggregates has been attempted over the years. For example, the kinetic approach, which is one of the representative approaches for prediction of dispersion state, describes time evolution of number density of various-sized aggregates by modeling the rate of fragmentation and aggregation between them [1]. For the establishment of these models, basic and quantitative understanding of aggregate dynamics in fluid flow has been required.

One of the most important issues is the interaction between fluid and aggregate, particularly the fragmentation process of aggregate under fluid stress. Many fragmentation models have been proposed from various point of view, in chronological order, the spherical model based on the balance between the internal strength and fluid stress[2], the model assuming two equal-sized spheres[3], the model considering the permeable fluid stress[4,5], the model considering the spatial variance of internal strength[6] , and so on. These models are based on the static balance of stresses and consequently they assumed that the fragmentation occurs immediately if the fluid stress exceeds the internal strength.

In the recent decade, many numerical studies on fluid–aggregate interaction have been performed. They have focused on the following three major topics, 1) fragmentation behavior, 2) fluid stress and internal strength, and 3) restructuring. The first topic concerns the dispersion behavior of an isolated aggregate in flow field. The relation between mass distribution of fragments and fluid stress has been discussed [7-10]. The second topic is regarding the fluid force and the resultant internal stress on a rigid (non-deformable) aggregate in fluid flow [11-15]. There have been a considerable number of researches on the dependence of the fluid force on the aggregate structure and the distribution of the inter-particle force of the aggregate with an open structure.

The last topic, the restructuring of an isolated aggregate by surrounding flow, usually represents the change in space-filling property of aggregate by fluid stress and sometimes indicates the microscopic change of bond distribution in the aggregate in the wider sense. Particularly the restructuring effect is enhanced in shear flow. In general, a soft matter in simple shear flow shows complicated structural change owing to both rotation and elongation effects of the flow field, even though it has a simple chain-like or string-like structure [16, 17]. There have been many numerical studies on the restructuring of aggregate in shear flow [18-24]. These

studies have reported that the magnitude relation between the bend stress by fluid force and the hold moment by inter-particle force is important for the restructuring of fractal aggregate. They have also revealed that the restructuring and the fragmentation of fractal aggregate take place simultaneously in the dispersion process and they are closely related to size distribution of consequent fragments. On the other hand, the restructuring of compact (non-fractal) aggregate has got less attention compared to that of fractal aggregate. However, the repetitive stress exerted on a rotating aggregate in shear flow brings about complicated changes in the bond network among particles. Consequently, the fragmentation behavior of aggregates varies widely even though they have similar space-filling properties [25, 26]. The knowledge of such restructuring processes of aggregate could be fed back to the kinetic models as a constitutive relation for the breakup process [27, 28].

The restructuring of non-fractal aggregate frequently occurs under the condition that the aggregate strength is comparable with the fluid stress. In simple shear flow, such a balance is characterized by the Fragmentation number Fa, which is the ratio of characteristic fluid stress to cohesive strength of aggregate. In general, when the shear stress is larger than the aggregate strength ($Fa \gg 1$), the aggregate immediately breaks up without restructuring. On the other hand, when the aggregate strength is larger than the shear stress ($Fa \ll 1$), no restructuring occurs because of the strong cohesion of aggregate. The successive restructuring is found for $Fa \sim 1$, when the cohesive strength of the aggregate is the same order of surrounding fluid stress. In such conditions, the aggregate deforms irreversibly with changing the internal structures from one state to another. Our previous studies [8,19] have suggested that the breakup of aggregate does not occur instantaneously because of the temporal change in internal structure, which is in contrast with the classic breakup models. However, quantitative models on the time-variation of the internal strength by restructuring have not been established.

In this study, the restructuring of a loose aggregate in simple shear flow was examined numerically. We performed a Lagrangian-type simulation of the behavior of a non-fractal aggregate in shear flow by Stokesian dynamics approach. The purpose of this study is to understand a detailed mechanism of the strength deterioration of aggregate and to elucidate the role of rotation and elongation effects of shear flow on it. Therefore we focus on the restructuring process for a specific condition that aggregate strength is comparable to fluid stress and discuss it through the comparison with the existing experimental results and theoretical models. We examine the structural change of aggregate from three different aspects. The first aspect is the

configuration change of aggregate. We investigate the detailed restructuring behavior through comparison of the configuration changes obtained from numerical and experimental results. The second aspect concerns the internal strength of aggregate. We examine the deterioration process of aggregate strength in fluid flow. The last is the fluid stress acting on the aggregate. We approximately calculate the fluid stress on the aggregate in order to understand the contribution of the fluid stress to the strength change of aggregate. Finally, we discuss the mechanism on strength deterioration of aggregate in simple shear flow comprehensively.

Numerical Methods

Stokesian dynamics

The motion of a particle aggregate in simple shear flow is calculated numerically by Stokesian dynamics approach. We applied the similar method to the original Stokesian dynamics analysis[29, 30]. The mobility matrix of particles is obtained from multiple expansion of Oseen tensor in Stokes flow and Faxèn's law. The external force, torque and the stresslet are related to the particle velocity, angular velocity and the rate of strain tensor of the undisturbed flow field by grand mobility matrix $\boldsymbol{M}$. The inverse of grand mobility matrix $\boldsymbol{M}^{-1}$ is expressed by component matrices in the following way.

$$\begin{pmatrix} \boldsymbol{F} \\ \boldsymbol{T} \\ \boldsymbol{S} \end{pmatrix} = \boldsymbol{M}^{-1} \begin{pmatrix} \boldsymbol{U} - \boldsymbol{u}^{\infty} \\ \boldsymbol{\Omega} - \boldsymbol{\Omega}^{\infty} \\ -\boldsymbol{E}^{\infty} \end{pmatrix}, \quad \boldsymbol{M}^{-1} = \begin{pmatrix} \boldsymbol{R}_{FU} & \boldsymbol{R}_{F\Omega} & \boldsymbol{R}_{FE} \\ \boldsymbol{R}_{TU} & \boldsymbol{R}_{T\Omega} & \boldsymbol{R}_{TE} \\ \boldsymbol{R}_{SU} & \boldsymbol{R}_{S\Omega} & \boldsymbol{R}_{SE} \end{pmatrix}, \tag{1}$$

where $\boldsymbol{F}$, $\boldsymbol{T}$ are the external force and torque acting on particles and $\boldsymbol{S}$ is stresslet. $\boldsymbol{U}$ and $\boldsymbol{\Omega}$ are the particle velocity and the angular velocity, $\boldsymbol{u}^{\infty}$, $\boldsymbol{\Omega}^{\infty}$ and $\boldsymbol{E}^{\infty}$ are the velocity, the angular velocity and the rate of strain tensor of undisturbed flow field, respectively. The velocity and the angular velocity of individual particles are calculated as

$$\begin{pmatrix} \boldsymbol{U} \\ \boldsymbol{\Omega} \end{pmatrix} = \begin{pmatrix} \boldsymbol{u}^{\infty} \\ \boldsymbol{\Omega}^{\infty} \end{pmatrix} + \begin{pmatrix} \overline{\boldsymbol{R}}_{FU} & \overline{\boldsymbol{R}}_{F\Omega} \\ \overline{\boldsymbol{R}}_{TU} & \overline{\boldsymbol{R}}_{T\Omega} \end{pmatrix}^{-1} \left[\begin{pmatrix} \boldsymbol{F} \\ \boldsymbol{T} \end{pmatrix} + \begin{pmatrix} \overline{\boldsymbol{R}}_{FE} \\ \overline{\boldsymbol{R}}_{TE} \end{pmatrix} : \boldsymbol{E}^{\infty} \right], \tag{2}$$

where $\overline{\boldsymbol{R}}$ is the modified resistance matrix considering lubrication effect and is obtained as follows;

$$\overline{\boldsymbol{R}} = \boldsymbol{M}^{-1} + \boldsymbol{R}_{2B} - \boldsymbol{M}_{2B}^{-1} \tag{3}$$

where $\boldsymbol{R}_{2B}$ is the resistance matrix for a pair of particles[31] and $\boldsymbol{M}_{2B}^{-1}$ is the inverse of the pair mobility matrix obtained in the same way as $\boldsymbol{M}^{-1}$. By numerical integration of Eq.(2), the instantaneous position of each particle is calculated.

The properties of primary particles and surrounding fluid are considered to be the same as those in our previous work [8]. We assumed that primary particles are perfectly smooth spheres with the diameter d (=2a) =650nm. For the physical properties of particle and fluid, those of polystyrene and ethanol are used. The particle and the fluid density are ρ_p=1056 kg/m^3, ρ_f=790 kg/m^3 respectively, and the fluid viscosity is μ=1.2×10^{-3} Pa·s. The inter-particle force is an attractive van der Waals force calculated from the retarded van der Waals potential based on the Lifshitz theory [32]. The corresponding non-retarded Hamaker constant is $A = 9.68\times10^{-21}$ J. If the distance between particles is smaller than the cut-off distance δ=1 nm, the inter-particle force acting on them is set equal to zero and any repulsive force is not given them. Even in this case, any overlap of particles does not occur owing to the lubrication force. We adopted very small time step because the inter-particle force exerted on closely-approaching particles is sensitive to the particle distance and consequently the selection of time step affects the relative motion of particle. The quantitative discussion on the setting of inter-particle force and the decision of time step have discussed in our previous article [8].

In this study, a tangential inter-particle force is not considered. It has been reported that the tangential force occasionally plays a significant role on the deformation of fractal aggregate [20, 21, 24]. Therefore the installation of tangential force model is possible to influence the simulation results on dynamic behaviors of a non-fractal aggregate as shown here. However, a physically-proved model on the tangential force has not been fully established in colloidal particulate system and the proposed models have undecided coefficients. Therefore we did not include the tangential force models in this simulation to avoid tuning parameters of the simulation results. Although we can not mention for certain about the effect of tangential force on the restructuring process of non-fractal aggregate at the present stage, the qualitative agreement between numerical and observation results shown later (Fig.3 and Fig.5) is a weak evidence of the less-significance of tangential force to the discussion given here.

In our simulation, inertias of both particle and fluid are neglected on the assumption that the particle is sufficiently small. On the other hand, in terms of the fact that Péclet number is sufficiently large, Brownian perturbation force is neglected. The justification of these assumptions can be also seen in our article [8].

The schematic diagram and the coordinate system of the calculation are shown in Fig.1. The surrounding flow field is simple shear flow, which consist of pure rotational flow and planar extensional flow which has the principal axes of stress along $y=x$ and $y=-x$. The undisturbed flow field is expressed by using the rotational velocity vector and the rate of strain tensor as follows;

$$\boldsymbol{u}^{\infty}(\boldsymbol{r}) = \boldsymbol{\Omega}^{\infty} \times \boldsymbol{r} + \boldsymbol{E}^{\infty} \cdot \boldsymbol{r} \tag{4}$$

$$\boldsymbol{\Omega}^{\infty} = -\frac{\dot{\gamma}}{2}\begin{pmatrix} 0 \\ 0 \\ 1 \end{pmatrix}, \quad \boldsymbol{E}^{\infty} = -\frac{\dot{\gamma}}{2}\begin{pmatrix} 0 & 1 & 0 \\ 1 & 0 & 0 \\ 0 & 0 & 0 \end{pmatrix}, \tag{5}$$

where $\dot{\gamma}$ is shear rate. By substituting Eqs.(4) and (5) into Eq.(2), the velocity and the angular velocity of particles are calculated. In Stokesian dynamics, the disturbed flow field due to the presence of particles is expressed by the mobility and the resistance matrices in Eqs.(1)-(3), which are functions of positions of each particle. In consequence, hydrodynamic interactions between particles can be considered in the simulation.

As shown in Fig.1, we use a spherical aggregate which has a loose structure as initial condition. It consists of a hundred primary particles and is made by the preliminary simulation of the collision process between a parent cluster and an isolated particle, which moves linearly from a random position to the parent cluster. The fractal dimension of initial aggregate is 3.0, which is evaluated from the relationship between the number of primary particles and the radius of gyration. The average coordination number is approximately 2.0. As is well-known, the coordination number is frequently used for describing the density of the contact-network among particles. However, it depends on evaluation method particularly in the case that each particle does not bond by physical contact. In this study, the coordination number is defined by the average number of particles existing within 2nm from each particle.

In our previous studies [8,19], we simulated the breakup behavior of aggregate in shear flow for a wide range of shear rate condition and reported the dependence of aggregate behaviors on the shear rate, i.e., the aggregate breaks up immediately for high shear rate, while it is hard to break up for low shear rate conditions. As mentioned in Introduction, the dispersion behavior is determined by Fragmentation number *Fa*, which is the ratio of characteristic fluid stress $\mu\dot{\gamma}$ to cohesive strength of aggregate σ. Here we focus on the deformation process before breakup in order to understand the deterioration of aggregate due to the successive

restructuring of constituent particles. Therefore we calculated the aggregate behavior in shear flow under the specific condition that the aggregate strength is comparable with fluid stress.

Quantitative evaluation of restructuring

In order to evaluate the restructuring of aggregate in flow field quantitatively, we attempt comparisons of simulation results with experimental and theoretical results of previous studies from various perspectives. The first attempt concerns configuration change of aggregate before breakup. Blaser [33] has performed the image analysis of successive pictures of aggregate behavior obtained from the experiment and has evaluated the deformation of aggregate in simple shear flow quantitatively. We apply the similar image analysis to the simulation results. We fit the outer shape of aggregate obtained from the visualization data of numerical simulation by a two-dimensional ellipse (see Fig.4a). By means of this analysis, our simulation results are compared to the experimental results quantitatively regarding the deformation of aggregate. The details of the analysis are described later.

The second attempt relates to the strength of aggregate. We evaluate the internal strength of aggregate caused by inter-particle force from the simulation results. As is well-known, Rumpf [34] has modelled cohesive strength of an aggregate on the assumption that an aggregate has homogeneous and isotropic structure and inter-particle force is constant in the following way.

$$\sigma = \frac{9}{8}\frac{\phi}{\pi d^2} kH \tag{6}$$

where d is the diameter of primary particle, ϕ is the volumetric concentration, k is the average coordination number and H is the inter-particle force.

In fact, previous studies have pointed out that the aggregate shows the irreversible deformation in fluid flow and it can not keep the initial structure in deformation process. The structural change caused by the deformation leads to the deterioration of internal strength of aggregate. Some researchers explained the fracture process in terms of crack growth in an aggregate [35-37]. However, the model for temporal change of the aggregate strength has not been proposed. In order to understand a mechanism of strength deterioration, we compare the simulation results with the existing model and investigate the change of internal strength of an aggregate in the deformation process.

The final attempt concerns the fluid stress acting on the aggregate. If the aggregate deforms and changes its outer shape, the fluid stress would change according to the instantaneous shape and the attitude of aggregate. In order to examine these effects, we calculate the fluid stress on the aggregate surface approximately. We fit a three-dimensional ellipsoid to the outer shape of aggregate obtained from simulation results. The previous studies[38, 39] calculated analytically the fluid stress on the ellipsoid in simple shear flow. We perform the similar analysis and evaluate the fluid stress on the surface of the ellipsoid fitted to the instantaneous aggregate shape. We calculate the fluid force acting on a fitted-ellipsoid on the basis of Jeffery's theory[38]. Under the assumption that inertias of both ellipsoid and fluid are small, the governing equation of fluid flow is given by Eq. (7) and Eq. (8).

$$\mu \Delta \boldsymbol{u} = \nabla p \tag{7}$$

$$\nabla \cdot \boldsymbol{u} = 0 \tag{8}$$

Disturbed flow field around the ellipsoid rotating with the surrounding flow is calculated by using the similar equation to Dirichlet equation which is used when one considers the gravitational potential. Solving Eq. (7) and Eq. (8), the hydrodynamic stress vector acting on the ellipsoidal surface is obtained as follows[38, 39];

$$\boldsymbol{f} = \left(- p_0 \boldsymbol{I} - 4\mu G \boldsymbol{I} + \frac{8\mu}{a_1 a_2 a_3} \boldsymbol{B} \right) \boldsymbol{n} \tag{9}$$

where $\boldsymbol{I}$ is unit matrix, a_1, a_2, a_3 are axes of ellipsoid, G and $\boldsymbol{B}$ are scalar and tensor constants which are functions of flow properties and geometric conditions of ellipsoid, and $\boldsymbol{n}$ is unit outward vector of ellipsoid. p_0 is ambient pressure and is set to be zero in our simulation.

Results and Discussion

Deformation behavior of aggregate

In the previous study [8], we simulated the behavior of a loose aggregate in shear flow for a wide range of shear rate. As described in Introduction, the purpose of this study is to elucidate the effect of surrounding fluid flow to the strength change of aggregate in detail. Here we focus on the aggregate behavior for a specific condition that the aggregate strength is comparable to the fluid stress. Figure 2 shows the numerical results on deformation behavior of aggregate in simple shear flow for $\mu\dot{\gamma}$=29.9 Pa. The spherical-shaped

aggregate slightly deforms with the rotation at an early stage and then it keeps almost constant shape. After several tens of rotations, it deforms again gradually and the restructuring of constituent particles occurs in the aggregate. The deformation process in the middle stage has two distinguishing features, i.e., the aggregate elongates with the streamline and then it bends into L-shape. In the later stage, the aggregate changes its shape irreversibly and then a small portion detaches itself from the parent aggregate. Finally the aggregate breaks up into two major child aggregates and one small portion.

Figure 3 (a) shows the details of deformation behavior in the middle stage obtained from numerical simulation. On the other hand, Fig.3 (b) shows the successive pictures of aggregate deformation obtained from the experiment by Blaser[33]. These figures show the motion of the aggregate at regular time intervals during one rotation period. The time-scale of the experimental and the simulation results in Fig.2 is different. However, it is well-known that a solid object placed in simple shear flow rotates one time in the period $4\pi/\dot{\gamma}$ for any shear rate $\dot{\gamma}$. In Fig.2, we compare both results per one cycle and therefore it corresponds to the same dimensionless time-scale $\dot{\gamma}t$. It can be seen in both results that the aggregate rotates with the deformation under the shear stress. As referred to in the previous article[8], even though the numerical conditions differ from experimental ones (the detailed experimental conditions can be found in his article[33]), these deformation behaviors are visually similar, i.e., the aggregate elongates along the streamline and bends when it turns to the direction normal to the streamline.

In order to evaluate the configuration change quantitatively, we performed the similar image analysis by Blaser. We extract the outer shape of aggregate on x–y plane (see Fig.1) and calculate the fitting of an ellipse to two-dimensional outer shape of aggregate. The deformation of aggregate was estimated from semi-major axis a and semi-minor axis b of the ellipse. The rotational attitude of aggregate is found from the angle α, which is defined as the angle between major axis of ellipse and x axis. Fig.4 (b) shows the time change in the ratio of semi-minor to semi-major axes of fitted ellipse b/a under the condition of $\mu\dot{\gamma} = 29.9$ Pa. This aspect ratio indicates the degree of deformation and it is unity if the aggregate keeps its initial spherical shape. As can be seen in Fig.4(b), the aspect ratio b/a changes periodically from 0.4 to 1.0 at the beginning and then it changes irreversibly. It indicates that the aggregate hardly keeps the spherical shape and changes its shape to the ellipsoidal one. These features are similar to the experimental observation[33]. The period of

small periodic change corresponds to the half period of a rotation $\dot{\gamma}t = 2\pi$, because the aggregate experiences twice compression/expansion per one rotation in simple shear flow.

Fig.4 (c) indicates the change of the angle α (the angle between major axis of fitted ellipse and x axis) with time. This angle represents the direction in which the aggregate deforms most. The linear change of α at early stages indicates that the aggregate rotates like a rigid body with constant rotational velocity. After the aggregate undergoes several rotations, the restructuring of particles begins to occur and the time change of α fluctuates gradually. The hillside-like change at later stages indicates that the aggregate elongates along the direction of streamline (α=180 deg.) and keep its direction for a certain period.

These deformation behaviors have been also found in the experiment. The experimental results indicated the stagnation of the rotation of ellipsoidal aggregate in the streamline. In order to understand the relation between the degree of deformation and the rotational attitude of aggregate, we examine the trajectory of the major axis of the fitted ellipse in accordance with the analysis by Blaser[33]. The trajectory of the semi-major axis at regular intervals is plotted in x'–y' plane in which all lengthscales are normalized by the projected area radius of ellipse. Figure 5 (a) shows our simulation results and (b) shows the experimental results by Blaser. It is found that the numerical and experimental results show very similar trajectories. The trajectory points are more frequent and slightly dispersed along x' axis (streamwise axis). These results indicate again that the aggregate elongate along the streamline with small rotational velocity. If the aggregate rotates with keeping spherical shape, these points trace on the circle with unit radius. However, both results indicate that the trajectory points trace on an ellipse and its major axis leans away from x' axis. The angle between the major axis of the orbital ellipse and x' axis is approximately 13 deg. (numerical results) and 6 deg. (experimental results). The direction shown by these angles is the direction in which the aggregate elongates most throughout the deformation process. It is found that most-elongated direction is close to the direction of streamline (0 deg.) although the direction of principal axis of the fluid stress is 45 deg. in shear flow. Blaser discussed this discrepancy and explained that the restructuring of particles leads to the retarded effect of the deformation[33].

Internal strength of aggregate

Most of previous studies have considered that the aggregate in fluid flow breaks up along the principle axis of fluid stress when the fluid stress is larger than the cohesive strength of aggregate which depends on the

internal structure of constituent particles. However, it is revealed that the internal structure of aggregate varies with time and the aggregate does not deform along the principal axis of fluid stress but along the streamline. In order to understand the restructuring effect on the aggregate strength, we investigate the change of the internal strength in the deformation process. The calculation method of internal strength from numerical results is as follows. The aggregate is divided into two parts along arbitrary cross-section in arbitrary direction. Then the cohesive force is estimated by summation of inter-particle force across the cross-section. On the other hand, the net cross-sectional area of the cut-end is calculated from the projected area in which the particles exist. By dividing the cohesive force by the cross-sectional area, we calculate the internal strength (stress) at each cross-section. From the above procedure, the weakest point of aggregate and the weakest direction, in which the weakest point reveals, are determined.

Figure 6 shows typical examples of distribution of internal strength in the weakest direction. Fig.6 (a) indicates the strength distribution of initial aggregate. Fig.6 (b) is the internal strength at the middle stage and (c) indicates the moment when the aggregate elongates along the streamline at the final stage. The direction of x'' axis indicates the weakest direction of the internal strength. The red lines in the figures indicate the cohesive strength calculated from Eq.(6) by substituting initial conditions of volumetric concentration ϕ, coordination number k and the resultant inter-particle force H. Fig.6 (a) indicates that initial aggregate has homogeneous distribution of internal strength and its average value is almost equal to the cohesive strength modelled by Rumpf [34]. On the other hand, the strength distributions of deformed aggregates are inhomogeneous and it entirely exceeds the Rumpf's model due to the periodic compression by shear flow (Fig.6b,c). These "tightening" behaviors of loose aggregate in fluid flow were reported in our previous study[8]. However, it is also found that the deformed aggregate has a local weak point in which the strength is lower than the predicted one by Rumpf's model. Because the constituent particles continuously stick to and separate from each other due to the periodic fluid stress, the weakest point varies with time and the strength in the aggregate declines gradually.

Figure 7 indicates the relation between the angle of major axis α and the angle of x'' direction against x axis for each instant of time. The former angle represents the most deformed direction while the latter is the weakest direction in the aggregate. It is found that there is a close correlation between these two directions. In most of previous models, it has been considered that an aggregate always break up in shear flow along the

principal axis of fluid stress. However, Fig.7 indicates the fact that the weak point inside aggregate always reveals in the direction of deformation. This result implies that the restructuring plays a crucial role on the strength deterioration of aggregate and the fragmentation occurs after complicated structural change inside the aggregate.

Fluid stress acting on aggregate

In previous fracture models, it has been assumed that initial (non-fractal) aggregate has spherical shape and the maximum fluid stress is exerted in the principle direction of fluid stress (45 and 225 deg. in shear flow). However, as described above, the numerical results show that the aggregate deforms irreversibly and it elongates along the flow direction rather than the principle direction. Consequently, the fluid stress on the aggregate surface would change with time since the outer shape of aggregate deviates from spherical one. In order to understand how the fluid force acting on the aggregate varies with time, we approximately calculate the distribution of fluid stress on the surface of aggregate by the similar method to Blaser's analysis [39]. We approximate the outer shape of deformed aggregate by an ellipsoid and calculate fluid stress acting on the surface of resultant ellipsoid on the basis of Jeffery's theoretical analysis [38]. The fitting procedure to ellipsoid is as follows. 1) We calculate the center of gravity of aggregate for each instant of time, 2) subtract it from positions of all constituent particles and calculate their relative positions, 3) divide the aggregate into small portions, 4) calculate the second moment (the volume integral of square sum of positions) of these portions with respect to an arbitrary axis for characterizing the spatial distribution of constituent particles, 5) define the axis which gives maximum values of the second moment as z''', 6) define the axis which is perpendicular to z''' and gives minimum value of the second moment as x''' and also define y''' axis normal to x''' and z''', 7) relate x'''–y'''–z''' coordinates to original x–y–z coordinates by using Euler angles φ, θ and ψ, and 8) calculate three axes of ellipsoid a_1, a_2 and a_3. Once we can obtain fitted ellipsoid by the above procedure, we calculate the fluid stress on the surface of ellipsoid from Eq.(9).

Figure 8 shows the distribution of fluid stress vectors on the surface of fitted ellipsoid. We show the fluid stress when the aggregate deforms in typical directions, i.e., (a) the aggregate deforms in principle axis of fluid stress (extension), (b) in flow direction, and (c) in principle axis of fluid stress (compression). It can be seen in the figures that the stress distribution varies with the shape and the posture of aggregate. These

complicated changes of fluid stress contribute to both deformation and rotational motion of aggregate. In case of a loose and deformable aggregate as considered here, the assumption of spherical shape is no longer applicable to the fracture model.

In order to understand the contribution of fluid stress on the aggregate motion in detail, we divide the ellipsoid into two equal-sized portions along x''' axis (the longest-side axis) and calculate the resultant fluid force acting on the semi-ellipsoid by integrating stress vectors. We decompose the fluid force vector to normal and tangential components so as to make clear the straining and rotating effects on the aggregate. Figure 9 shows (left) total fluid force, (center) normal component and (right) and tangential component of fluid force acting on aggregate (semi-ellipsoids). Figures (a) to (j) indicate the configuration of aggregate at regular time intervals at the final stage of restructuring. When the long axis of deformed aggregate directs toward the principle axes of fluid stress, the fluid force vector also directs toward them and it contribute only the deformation (no tangential component). On the other hand, the tangential component of fluid force is significant when the aggregate deforms toward flow direction. These tangential forces bring about the irregular rotational motion of aggregate shown in Fig.4(c).

The relation between the instantaneous attitude of deformed aggregate and fluid force is examined. We project the first axis of fitted ellipsoid a_1 on $x-y$ plane and define the angle between a_1 and x axis as α_{vol}. The angle α_{vol} indicates inclination angle of ellipsoid and it is distinguished from α in Fig.4, which is the inclination angle of two-dimensional fitted ellipse. However, there is no significant difference between them because the aggregate scarcely incline in z direction.

Figure 10 shows the normal component of fluid force F_n and the fluid torque T_z about z axis, which is calculated from the tangential component of fluid force F_t exerted on the fitted ellipsoid, at various angles. The results are normalized by the maximum fluid force exerted on a sphere with equivalent volume radius R_{sphere} in simple shear flow described as follows.

$$\left|F_{\mathrm{sphere}}\right| = \frac{5}{2}\pi\mu\dot{\gamma}R_{\mathrm{sphere}}^2 \tag{10}$$

It is found from Fig.10(a) that the normal component of fluid force F_n, which contributes to the deformation of aggregate, is exerted in compression direction at angles $-90\,\mathrm{deg.} \le \alpha_{\mathrm{vol}} \le 0\,\mathrm{deg.}$ and is exerted in tensile direction at $0\,\mathrm{deg.} \le \alpha_{\mathrm{vol}} \le 90\,\mathrm{deg.}$ as are expected. When the aggregate does not deform so much and it

almost keeps a spherical shape at the early stage, the fluid force F_n is exerted synchronized with the rotation and its magnitude is almost the same as F_{sphere}. However, at the final stage when the aggregate deforms significantly, F_n is exerted irregularly on the aggregate in a wide range of α_{vol}. It means that the tensile force continues to act on the aggregate until the aggregate elongates along the streamline after it passes through the principal axis of tensile stress. Such a complicated variance of fluid force would be one of the reasons for "retarded effect" of aggregate deformation which is described in Fig.5.

Figure10 (b) shows the fluid torque T_z exerted on the fitted ellipsoid at various angles α_{vol}. As can be seen in Fig.10(b), the fluid torque exerts in the clockwise direction at angles $-90\,\mathrm{deg.} \le \alpha_{\mathrm{vol}} \le -45\,\mathrm{deg.}$ and $45\,\mathrm{deg.} \le \alpha_{\mathrm{vol}} \le 90\,\mathrm{deg.}$, while it exerts in counter clockwise direction at $-45\,\mathrm{deg.} \le \alpha_{\mathrm{vol}} \le 45\,\mathrm{deg.}$ These results indicate that, when the aggregate turns to the direction normal to the streamline, the torque is exerted in the direction coincident with the rotation and consequently the rotational velocity increases. On the other hand, the fluid torque suppresses the rotation when the aggregate elongates along the streamline and it results in the stagnation of rotation. The hillside-like change of the inclination angle at later stages, which is indicated in Fig.4(c), can be explained by these results on fluid torque.

Strength deterioration of aggregate

From the results in the above section, it is found that the strength deterioration of aggregate in flow is caused by complicated interactions between the deformation of aggregate and the fluid force acting on it. In other words, the fluid force changes the aggregate shape, while the shape change brings about the fluid force change. In order to quantify such interactions, we relate the instantaneous aggregate shape to the fluid force acting on it. Figure 11 indicates the relation between second moment of fitted ellipsoid along with x''' direction (long-side axis of ellipsoid) and normal component of fluid force which contributes to the deformation throughout the deformation process. The second moment is normalized by that exerted on a sphere with equivalent volume radius R_{sphere} as follows.

$$M_{\mathrm{sphere}} = \frac{2}{5} V_{\mathrm{el}} R_{\mathrm{sphere}}^2 \tag{11}$$

where V_{el} is the instantaneous volume of fitted ellipsoid. In Fig.11, $M_{x'''}/M_{sphere}=1$ indicates that the aggregate has a spherical shape and the smaller value indicates an elongated shape. On the other hand, $F_n/|F_{sphere}|=\pm 1$ indicate that tensile and compression forces acting on the aggregate is the same as those on a corresponding sphere (Eq.(10)). The plots in Fig.11 are separated for each rotation period of aggregate. If the soft object deforms reversibly in shear flow, the plot for each cycle is closed and the elliptical trajectory can be obtained.

In the early period (the 1st to 4th period), the trajectory cycle is closed, i.e., the aggregate deforms but it can return to the original shape. The reason why the normal component of fluid force F_n does not reach $|F_{sphere}|$ is that, even though the aggregate has almost a spherical shape, the long axis of fitted ellipse x''' does not always locate on x–y plane because of non-biased nature of the shape. After the 5th period, the second moment decreases with the increase of rotation number although the absolute value of maximum fluid force is approximately constant. These results indicate that the deformation behavior becomes irreversible. These features are characteristic for shear flow in which the aggregate is subject to the tensile and compressing forces periodically with its rotation. Such periodical forces of tension and compression bring about continuous restructuring of primary particles and consequently the strength deterioration inside aggregate developed toward its fracture.

Conclusion

The strength deterioration of non-fractal aggregate in simple shear flow was investigated numerically. Particularly we focused on the strength change of a loose aggregate under the condition that the internal strength is comparable to surrounding fluid stress. The deformation behaviors of aggregate obtained from the simulation are similar to the experimental results, i.e., the aggregate elongates along the streamline, not along the principal axes of fluid stress. We examined the structural change of aggregate with respect to the outer shape, the internal strength and the fluid stress exerted on the aggregate. It is found that the retarded effect of deformation brings about the successive restructuring. The weak point gradually develops in the aggregate by the restructuring and the aggregate finally ruptures at the weak point. The internal strength of aggregate is complexly affected by combination of rotation and elongation effect of shear flow. It is concluded that the

structural change of aggregate in shear flow has highly irreversible features.

Acknowledgment

The authors would like to thank Mr. Manabu Sawada and Mr. Hiroo Nogami (Murata Manufacturing Co., Ltd.) for helpful contribution to the calculation of inter-particle force.

References

(1) Smoluchowski M. Versuch einer Machematischen Theorie der Koagulationskinetik Kolloider Löesungen. *Z. Phys. Chem.* **1917**, *92*, 129-168.

(2) Bagster D.F.; Tomi D. The Stresses within a Sphere in Simple Flow Fields. *Chem. Eng. Sci.* **1974**, *29*, 1773-1783.

(3) Zeichner G.R.; Schowalter W.R. Use of Trajectory Analysis to Study Stability of Colloidal Dispersions in Flow Fields. *AIChE J.* **1977**, *23*, 243-254.

(4) Adler P.M.; Mills P.M. Motion and Rupture of a Porous Sphere in a Linear Flow Field. *J. Rheology* **1979**, *23*, 25-37.

(5) Sonntag R.C.; Russel W.B. Structure and Breakup of Flocs Subjected to Fluid Stresses: II. Theory. *J. Colloid Interface Sci*. **1987**, *115*, 378-389.

(6) Horwatt S.W.; Manas-Zloczower I.; Feke D.L. Dispersion Behavior of Heterogeneous Agglomerates at Supercritical Stresses. *Chem. Eng. Sci.* **1992**, *47*, 1849-1855.

(7) Higashitani K.; Iimura K.; Sanda H. Simulation of Deformation and Breakup of Large Aggregates in Flows of Viscous Fluids. *Chem. Eng. Sci.* **2001**, *56*, 2927-2938.

(8) Harada S.; Tanaka R.; Nogami H.; Sawada M. Dependence of Fragmentation Behavior of Colloidal Aggregates on Their Fractal Structure. *J. Colloid Interface Sci*. **2006**, *301*, 123-129.

(9) Harshe Y.M.; Lattuada M. Breakage Rate of Colloidal Aggregates in Shear Flow through Stokesian Dynamics. *Langmuir* **2012**, *28*, 283-292.

(10) Nishiyama T.; Inamuro T.; Yasuda S. Numerical Simulation of the Dispersion of Aggregated Brownian Particles under Shear Flows. *Comp. Fluids* **2013**, **86**, 395-404.

(11) Harshe Y.M.; Ehrl L.; Lattuada M. Hydrodynamic Properties of Rigid Fractal Aggregates of Arbitrary Morphology. *J. Colloid Interface Sci*. **2010**, *352*, 87-98.

(12) Seto R.; Botet R.; Briesen H. Hydrodynamic Stress on Small Colloidal Aggregates in Shear Flow using Stokesian Dynamics. *Phys. Rev. E* **2011**, *84*, 041405.

(13) Gastaldi A.; Vanni M. The Distribution of Stresses in Rigid Fractal-like Aggregates in a Uniform Flow Field. *J. Colloid Interface Sci*. **2011**, *357*, 18-30.

(14) Schlauch E.; Ernst M.; Seto R.; Briesen H.; Somerfeld M.; Behr M. Comparison of Three Simulation Methods for Colloidal Aggregates in Stokes Flow: Finite Elements, Lattice Boltzmann and Stokesian Dynamics. *Comp. Fluids* **2013**, *86*, 199-209.

(15) Fellay L.S.; Twist C.; Vanni M. Motion of Rigid Aggregates under Different Flow Conditions. *Acta, Mech.* **2013**, *224*, 2225-2248.

(16) Zia I.Y.Z.; Cox R.G.; Mason S.G. Ordered Aggregates of Particles in Shear Flow. *Proc. R. Soc. A* **1967**, 300, 421-441.

(17) Schroeder C.M.; Rodrigo E.T.; Shaqfeh E.S.G.; Chu S. Characteristic Periodic Motion of Polymers in Shear Flow. *Phys. Rev. Lett.* **2005**, *95*, 018301.

(18) Potanin A.A. On the Computer Simulation of the Deformation and Breakup of Colloidal Aggregates in Shear Flow. *J. Colloid Interface Sci*. **1993**, *157*, 399-410.

(19) Harada S.; Tanaka R.; Nogami H.; Sawada M.; Asakura K. Structural Change in Non-fractal Particle Clusters under Fluid Stress. *Colloids Surf. A* **2007**, *302*, 396-402.

(20) Becker V.; Schlauch E.; Behr M.; Briesen H. Restructuring of Colloidal Aggregates in Shear Flows and Limitations of the Free-draining Approximation. *J. Colloid Interface Sci*. **2009**, *339*, 362-372.

(21) Becker V.; Briesen H. A Master Curve for the Onset of Shear Induced Restructuring of Fractal Colloidal Aggregates. *J. Colloid Interface Sci*. **2010**, *346*, 32-36.

(22) Eggersdorfer M.L.; Kadau D.; Herrmann H.J.; Pratsinis S.E. Fragmentation and Restructuring of Soft-agglomerates under Shear. *J. Colloid Interface Sci*. **2010**, *342*, 261-268.

(23) Vanni M.; Gastaldi A. Hydrodynamic Forces and Critical Stresses in Low-Density Aggregates under Shear Flow. *Langmuir*, **2011**, *27*, 12822-12833.

(24) Seto R.; Botet R.; Auernhammer G.K.; Briesen H. Restructuring of Colloidal Aggregates in Shear Flow. *Eur. Phys. J. E* **2012**, *35*, 128-139.

(25) Bäbler, M.U.; Morbidelli, M.; Bałdyga, J. Modelling the Breakup of Solid Aggregates in Turbulent Flows. *J. Fluid Mech.* **2008**, *612*, 261-289.

(26) Zaccone A.; Soos M.; Lattuada M.; Wu H.; Bäbler M.U.; Morbidelli, M. Breakup of Dense Colloidal Aggregates under Hydrodynamic Stresses. *Phys. Rev. E* **2009**, *79*, 061401.

(27) Gmachowski L. Aggregate Restructuring and Its Effect on the Aggregate Size Distribution. *Colloids Surf. A* **2002**, *207*, 271-277.

(28) Selomulya C.; Bushell G.; Amal R.; Waite T.D. Understanding the Role of Restructuring in Flocculation: The Application of a Population Balance Model. *Chem. Eng. Sci.*, **2003**, *58*, 327-338.

(29) Brady J.F.; Bossis G. Stokesian Dynamics. *Ann. Rev. Fluid Mech*. **1988**, *20*, 111-157.

(30) Durlofsky L.; Brady J.F.; Bossis G. Dynamic Simulation of Hydrodynamically Interacting Particles. *J. Fluid Mech*. **1987**, *180*, 21-49.

(31) Jeffery D.J.; Onishi Y. Calculation of the Resistance and Mobility Functions for Two Unequal Rigid Spheres in Low-Reynolds-number Flow. *J. Fluid Mech*. **1984**, *139*, 261-290.

(32) Bowen W.R.; Jenner F. The Calculation of Dispersion Forces for Engineering Applications. *Adv. Colloid Interface Sci*. **1995**, *56*, 201-243.

(33) Blaser S. Flocs in Shear and Strain Flows. *J. Colloid Interface Sci*. **2000**, *225*, 273-284.

(34) Rumpf H. Zur Theorie der Zugfestigkeit von Agglomeraten bei Kraftübertragung an Kontaktpunkten. *Chem. Ing. Tech.* **1970**, *42*, 538-540.

(35) Kendall K. Agglomerate Strength. *Powder Metall.* **1988***, 31,* 28-31.

(36) Vassileva N.D.; van den Ende D.; Mugele F.; Mellema J. Restructuring and Break-up of Two-dimensional Aggregates in Shear Flow. *Langmuir*, **2006**, *22*, 4959-4967.

(37) Harshe Y.M.; Lattuada M.; Soos M. Experimental and Modeling Study of Breakage and Restructuring of Open and Dense Colloidal Aggregates. *Langmuir*, **2011**, *27*, 5739-5752.

(38) Jeffery G.B. The Motion of Ellipsoidal Particles Immersed in a Viscous Fluid. *Proc. R. Soc. Lond. A* **1922**, *102*, 161-179.

(39) Blaser S. Forces on the Surface of Small Ellipsoidal Particles Immersed in a Linear Flow Field. *Chem. Eng. Sci*. **2002**, *57*, 515-526.

Figure list

Figure 1: Schematic diagram of calculation system.

Figure 2: Instantaneous motion of aggregate on x–y plane in steps of normalized time $\dot{\gamma}t = 18.9$.

Figure 3: Rotation and deformation of aggregate in simple shear flow for one cycle. Time passes from left to right. (a) simulation results and (b) experimental results[33].

Figure 4: Time change in geometric quantities of fitted ellipse; (a) definition of geometric variables, (b) aspect ratio b/a and (c) inclination angle of major axis α.

Figure 5: Trajectory of normalized semi-major axis of ellipse; (a) simulation results and (b) experimental results[33] (x and y axes in Fig.(b) correspond to x' and y' respectively).

Figure 6: Distribution of internal stress of aggregate; (a) initial condition, (b) middle stage and (c) final stage of deformation process (x'': weakest direction).

Figure 7: Relation between deformed direction (inclination angle of fitted ellipse α) and weakest direction (angle between x and x'' axes).

Figure 8: Distribution of fluid stress on the surface of ellipsoid. (a) deform along $y=x$ ($\dot{\gamma}t = 164.5$), (b) deform along x axis ($\dot{\gamma}t = 173.25$) and (c) deform along $y = -x$ ($\dot{\gamma}t = 176.75$).

Figure 9: Fluid force acting on aggregate at the final stage of restructuring; (left) total force, (center) normal component and (right) tangential component.

Figure 10: Force and torque acting on aggregate caused by fluid stress.

Figure 11: Relation between normal component of fluid force and second moment of ellipsoid.

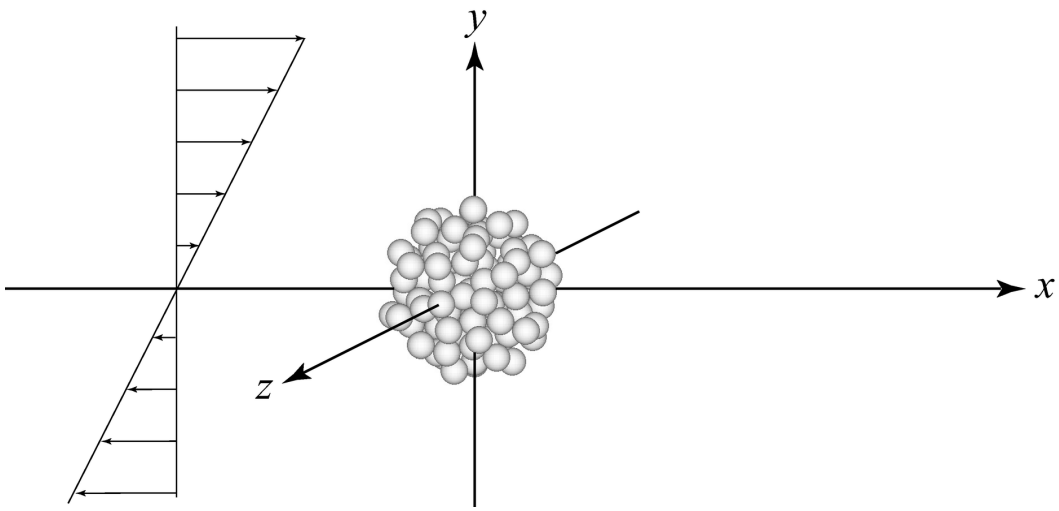

Figure 1: Schematic diagram of calculation system.

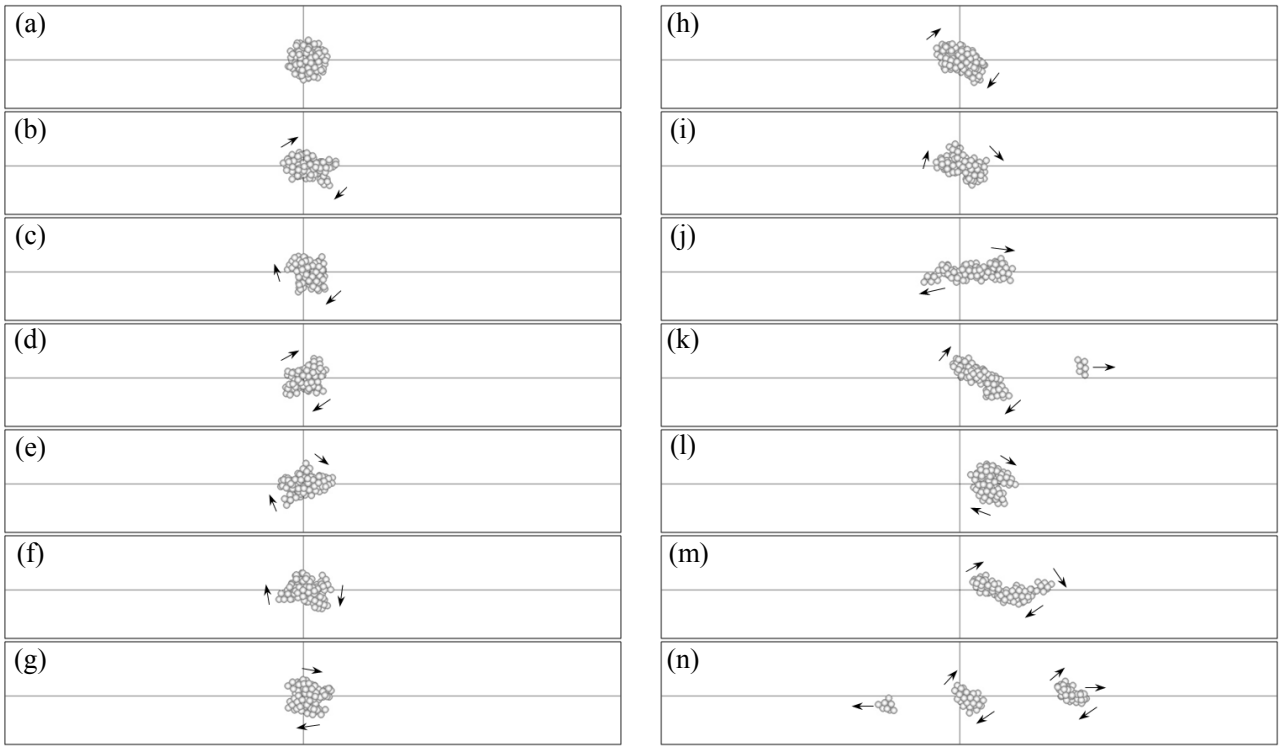

Figure 2: Instantaneous motion of aggregate on x–y plane in steps of normalized time $\dot{\gamma}t = 18.9$.

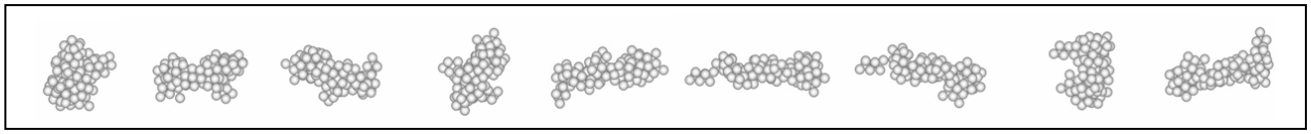

(a) simulation results

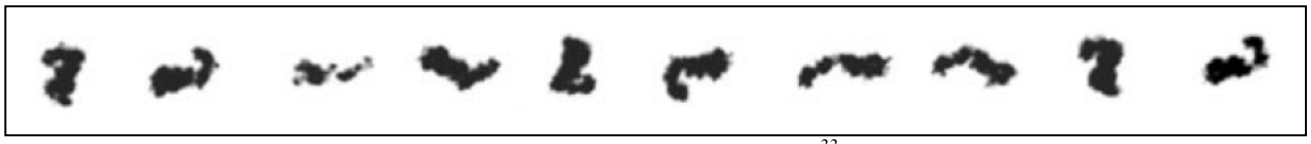

(b) experimental results by Blaser[33]

Figure 3: Rotation and deformation of aggregate in simple shear flow for one cycle. Time passes from left to right. (a) simulation results and (b) experimental results[33].

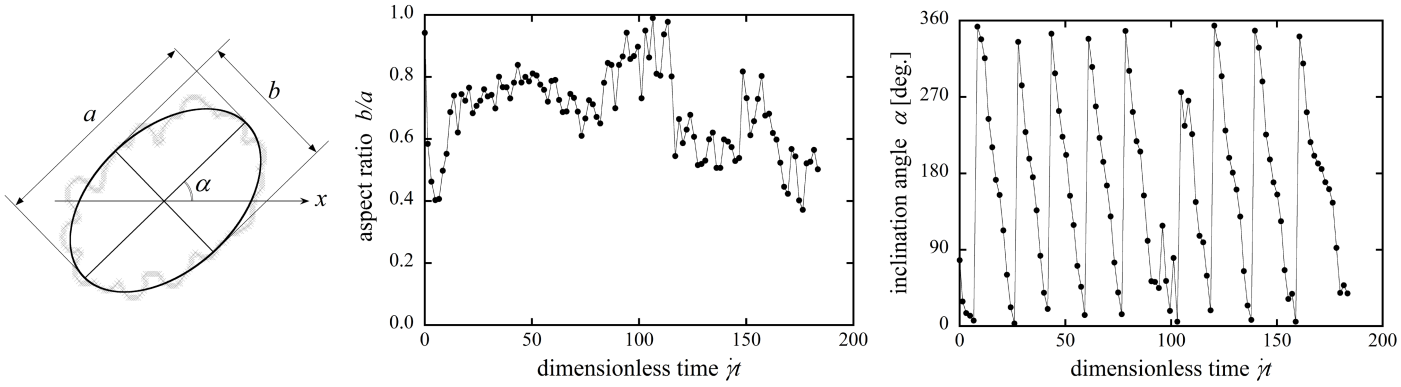

(a) geometric variables (b) aspect ratio (c) inclination angle

Figure 4: Time change in geometric quantities of fitted ellipse; (a) definition of geometric variables, (b) aspect ratio b/a and (c) inclination angle of major axis α.

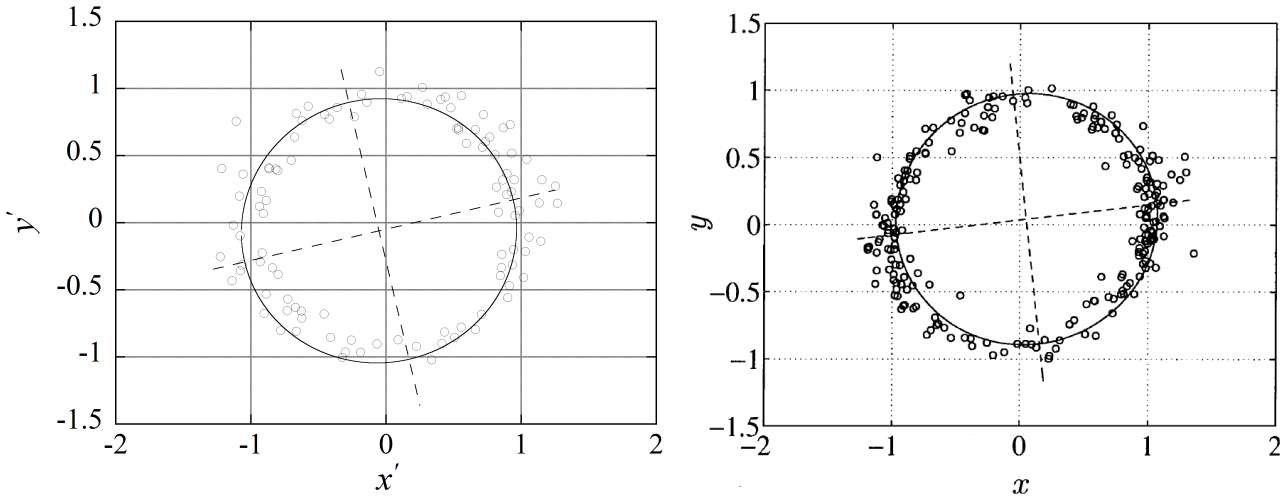

(a) simulation results (b) experimental results[3]

Figure 5: Trajectory of normalized semi-major axis of ellipse; (a) simulation results and (b) experimental results[33] (x and y axes in Fig.(b) correspond to x' and y' respectively).

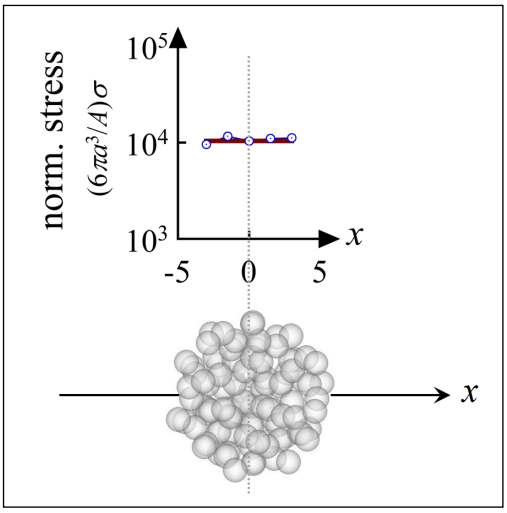

(a) initial condition ($\dot{\gamma}t = 0$)

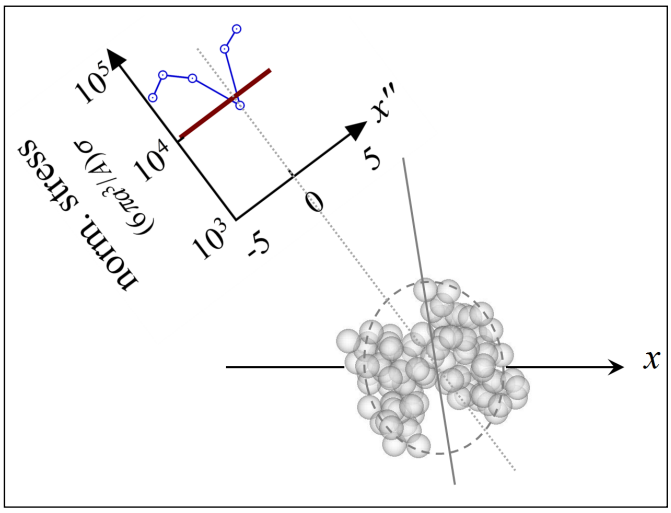

(b) middle stage ($\dot{\gamma}t = 115.15$)

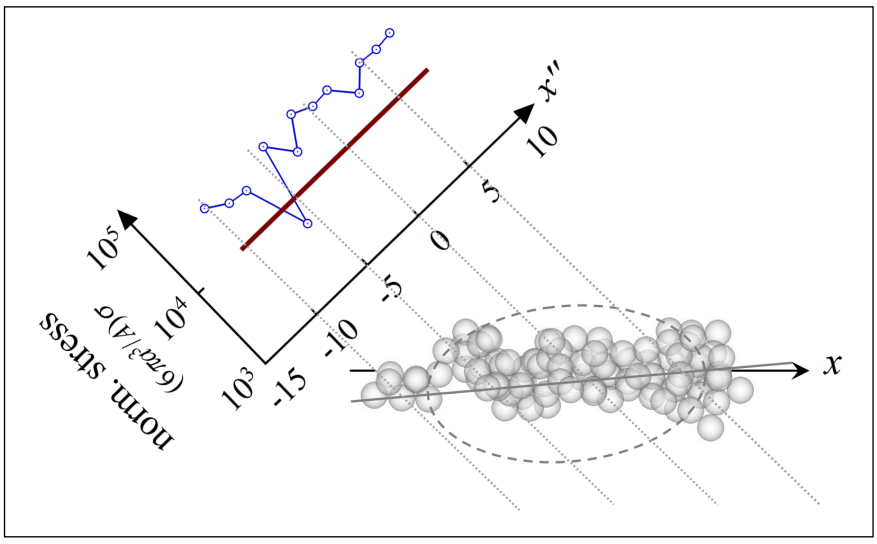

(c) final stage ($\dot{\gamma}t = 171.15$)

Figure 6: Distribution of internal stress of aggregate; (a) initial condition, (b) middle stage and (c) final stage of deformation process (x'': weakest direction).

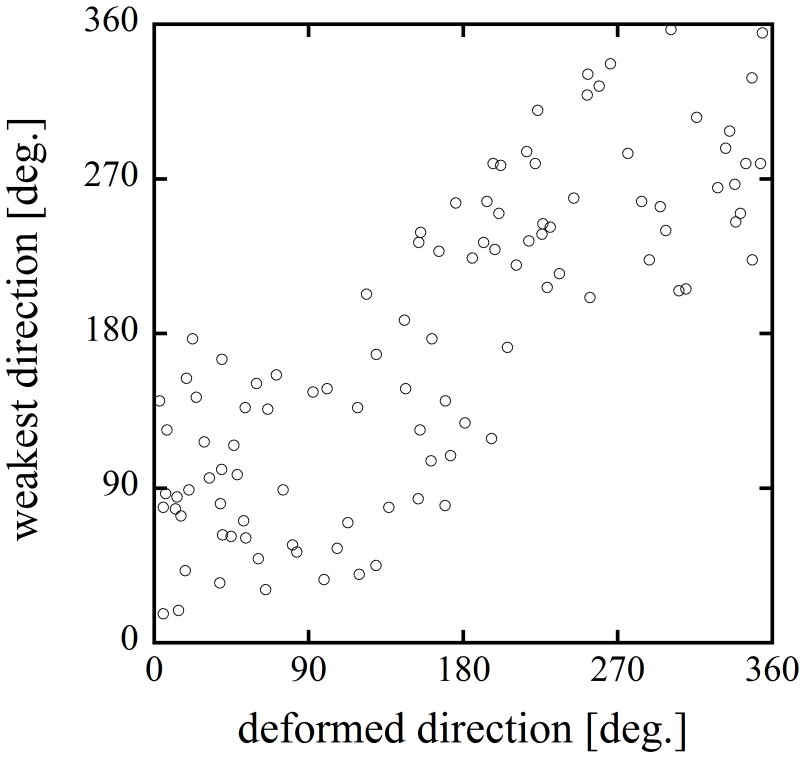

Figure 7: Relation between deformed direction (inclination angle of fitted ellipse α) and weakest direction (angle between x and x'' axes).

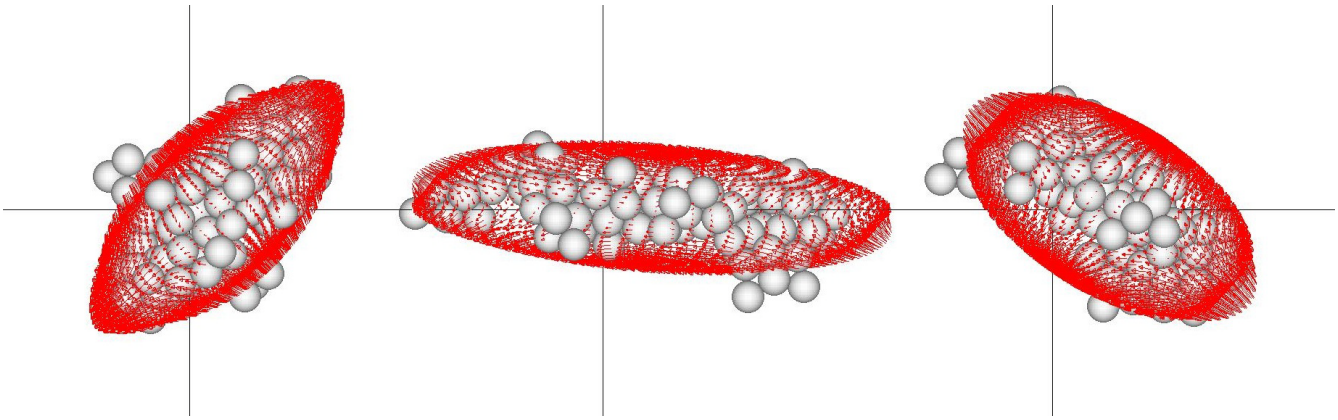

(a) deformed along $y=x$ (b) deformed along x axis (c) deformed along $y=-x$

Figure 8: Distribution of fluid stress on the surface of ellipsoid. (a) deform along $y=x$ ($\dot{\gamma}t=164.5$), (b) deform along x axis ($\dot{\gamma}t=173.25$) and (c) deform along $y=-x$ ($\dot{\gamma}t=176.75$).

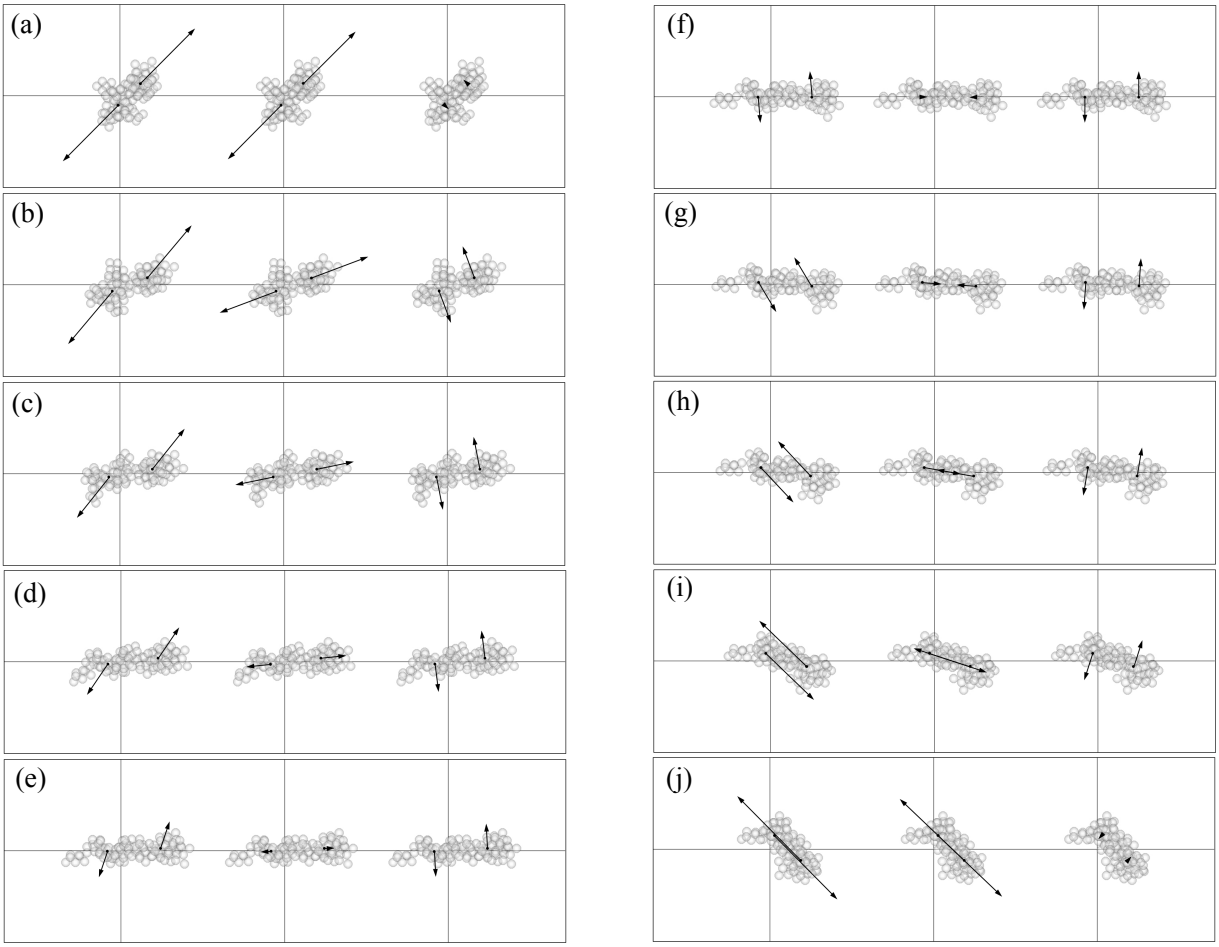

Figure 9: Fluid force acting on aggregate at the final stage of restructuring; (left) total force, (center) normal component and (right) tangential component.

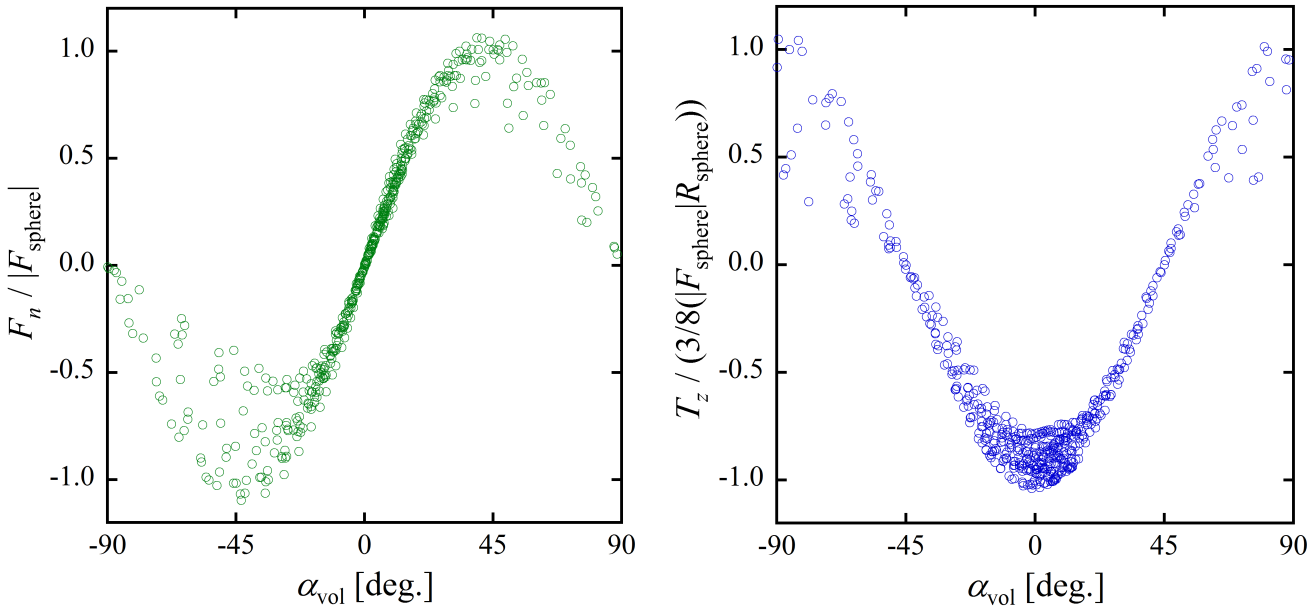

(a) fluid force (positive: tension) (b) fluid torque (positive: clockwise)

Figure 10: Force and torque acting on aggregate caused by fluid stress.

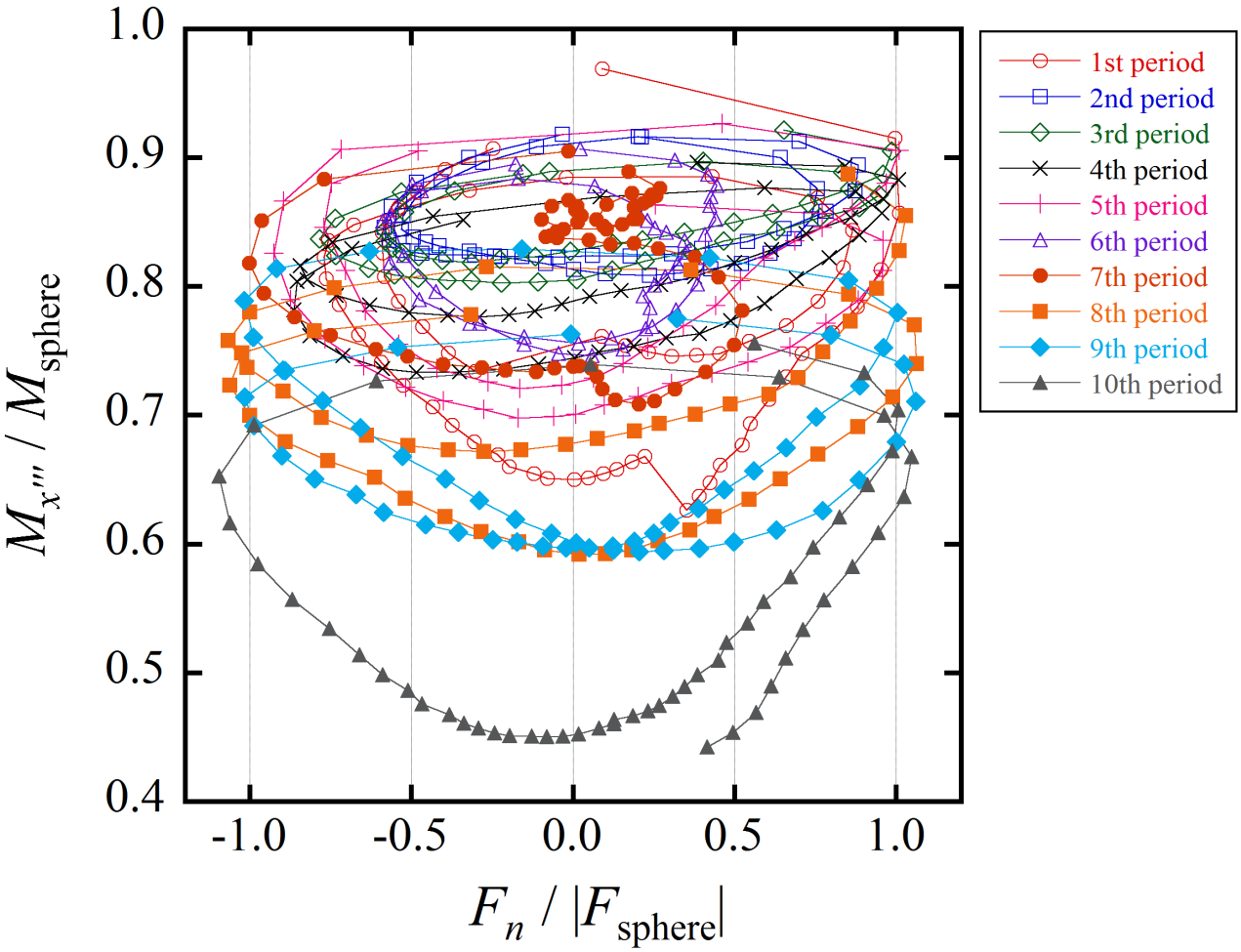

Figure 11: Relation between normal component of fluid force and second moment of ellipsoid.

TOC Graphic